



Time response of the thin layer electrochemical cell used for in situ X-ray diffraction

J.E. DeVilbiss^{a,*}, J.X. Wang^b, B.M. Ocko^c, K. Tamura^c, R.R. Adzic^c,
I.A. Vartanyants^a, I.K. Robinson^a

^a Department of Physics, University of Illinois, Urbana, IL 61801, USA

^b Brookhaven National Laboratory, Energy Science and Technology Department, Upton, NY 11973, USA

^c Brookhaven National Laboratory, Department of Physics, Upton, NY 11973, USA

Received 30 May 2001; received in revised form 14 March 2002

Abstract

As the potential applied to the bromide on Ag(001) thin layer electrochemical cell increases past a critical level, the bromide adlayer undergoes a second order phase transition from a disordered state to an ordered state. Using surface X-ray diffraction we measured the time response of this phase transition due to an applied step potential. We find that the time response of the phase transition is limited by the properties of the thin layer geometry. By modeling the electrochemical cell as a RC circuit, we argue that the observed time delay is primarily due to the slow diffusion of charge into the central region of the electrode surface. Crown Copyright © 2002 Published by Elsevier Science Ltd. All rights reserved.

Keywords: Phase transition; Thin layer cell; Surface ordering; Time response; Diffusion equation

1. Introduction

Adsorbed species on an electrode surface can undergo both first and second order phase transitions as a function of the applied potential. The structure of these phases can be ascertained from both scanning probe and X-ray scattering techniques. However, much less is known about the kinetics of these phase transitions. For scanning probe measurements, the kinetic behavior is strongly influenced by the confinement of the sample under the scanning tip. With X-ray measurements the time response of the electrode is influenced by the characteristics of the ‘thin layer cell’ geometry in which the electrolyte region is only a few microns thick. This geometry has provided a compromise between the conflicting needs of (a) maintaining electrochemical equilibrium and (b) minimizing the absorption in and scattering from the electrolyte. This study has been conducted, in part, to gauge the effectiveness of the thin

layer geometry for measuring the kinetics of phase transitions. In particular we have observed and modeled the inherent time dependent response of the thin layer geometry arising from the internal resistance and capacitance of the cell.

The electrochemical deposition of bromide on Ag(001) has previously been described as the deposition of adsorbates into a square lattice of substrate sites [1]. The energetics of this system may be modeled by the ‘Ising’ model Hamiltonian, $H = J \sum_{i,j} n_i n_j - \mu \sum_i n_i$, where J is a lateral interaction parameter, μ is the electrochemical potential, and the first sum is taken over nearest neighbors on a square lattice [2]. The model is isomorphic to the Ising spin ($s = 1/2$) model in two dimensions and predicts a second order phase transition as the applied potential increases past a critical value [1].

The bromide ions are adsorbed on hollow sites of the underlying square lattice (Fig. 1). Adjacent sites in the lattice cannot be occupied because the bromide ion is larger than the silver atom. Consequently the bromide lattice may occupy one of two possible $\sqrt{2} \times \sqrt{2}$ sublattices. At low potentials, the system is characterized by a long-range disorder with domains of small size being randomly and equally distributed between the two sub-

* Corresponding author. Tel.: +1-217-333-7382; fax: +1-217-244-2278

E-mail address: devilbss@uiuc.edu (J.E. DeVilbiss).

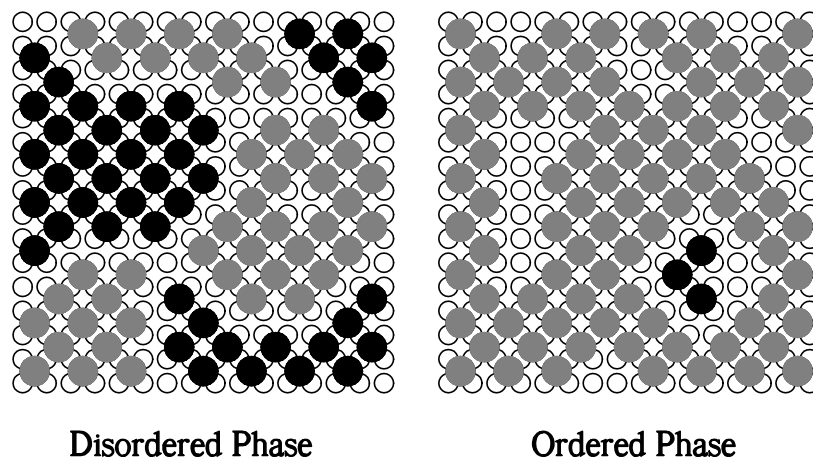


Fig. 1. Real space sketch of the Ag(001) surface (hollow circles). Relative to the body-centered-tetragonal conventional unit cell, a lattice gas of bromide atoms (filled circles) forming small domains of $c(2 \times 2)$ structures are shown in a phase exhibiting long-range disorder (left) and in a phase exhibiting long-range order (right). The black solid circles and the gray solid circles respectively correspond to bromide atoms on the two different sub-lattices. Note that even in the ordered phase, there are small domains which lie on the minority sub-lattice. Such a domain is seen in the lower right of the ordered phase sample.

lattices. As the applied potential increases, the average domain size increases. Above a critical potential the average domain size will be on the order of the size of the entire system (typically a facet size) so that one of the two sub-lattices will have a majority occupation. This spontaneous symmetry breaking distinguishes the ordered phase of the system.

The order–disorder phase transition may be directly monitored by measuring the X-ray scattering intensity from the surface at specific locations in the reciprocal space [1]. Relative to the body-centered tetragonal conventional unit cell, the $(1, 0, L)$ truncation rod [3,4] arises from the underlying silver lattice. As the adlayer coverage increases (irrespective of ordering), the intensity of this rod decreases. On the other hand, the $(1/2, 1/2, L)$ rod corresponds to a long-range domination of one of the two domain types. The scattered intensity (S) of the $(1/2, 1/2, L)$ rod is predicted to scale as the square of the Ising order parameter: $S \propto (V - V_c)^{2\beta}$ for $V > V_c$ [1,2], where V_c is the critical potential. The solution of the two dimensional- (2D) Ising model on a square lattice predicts an exponent $\beta = 1/8$ [5,6]. Past observations are consistent with the $\beta = 1/8$ value close to the transition but deviate from this form far from the transition [1]. Although the exponent is universal, the critical potential is not and depends on concentration.

Similar diffraction pattern changes have been used by Finnefrock et al. to study the kinetics of the electro-deposition of Cu–Cl on the Pt(111) surface near an order-disorder phase transition [7]. They have attributed the kinetic behavior of this system primarily to the nucleation and growth of 2D islands rather than to the limitations of the thin-layer cell geometry. However, there is a significant difference between the Cu–Cl on Pt(111) phase transition and the Br on Ag(001) phase

transition. The Cu–Cl on Pt(111) phase transition is first order and is immediately preceded by a discontinuous change in coverage. The bromide on Ag(001) phase transition, in contrast, is second order and may, therefore, be much faster. In this paper, we present results for the kinetics of the electroadsorption of Br on Ag(001). Our results indicate that the observed time-dependent transition is primarily governed by the properties of the thin layer geometry of the electrochemical cell.

2. Experimental methods

We prepared an electrochemical cell of Ag(001) in a thin layer of 1 M NaClO₄ and 10 mM KBr solution (pH \sim 10). We used a Ag(001) single crystal of radius $R = 4.0$ mm which was oriented within 0.2° of the (001) crystallographic plane. The crystal was chemically polished using a CrO₃/HCl solution. After the crystal was cleaned in concentrated sulfuric acid and pure water, the sample surface was covered by a drop of water and transferred into the electrochemical X-ray scattering cell. We then used a 6 μ m polypropylene film to seal the cell. Excess solution was drained from the cell so that a thin capillary film of electrolyte remained between the crystal and the polypropylene film. We flushed an outer chamber with N₂ gas to prevent oxygen from diffusing through the polypropylene membrane [8]. In units of the body-centered-tetragonal conventional unit cell ($a = b = 2.889$ Å, $c = 4.086$ Å) we monitored the surface X-ray diffraction. The observations were made at beam line X22A of the National Synchrotron Light Source (NSLS) at Brookhaven National Laboratory using a four-circle diffractometer. Diffraction positions were selected using the symmetric $\omega = 0$ geometry. The focused incident beam was square in shape with dimen-

sions (0.5×0.5 mm). This beam was diffracted from the center of the sample when the steady-state response of the cell was being studied. When the time response of the cell was being monitored, the beam was diffracted from the sample at an off-center position. We estimated this radius as $r = 3.5$ mm.

The steady state response of the cell was determined by measuring the intensity of the $(1/2, 1/2, L)$ rod at $L = 0.05$ as the potential applied at the Ag sample (relative to the $[\text{Ag}/\text{AgCl}]$ reference electrode) swept from -0.4 to -0.8 V with steps of 0.01 V. The intensity at each potential in this range was measured for 10 s to allow the system to approach a steady state. The scan direction was then reversed to observe the hysteresis of the transition.

In order to observe the time dependence of the phase transition, we applied four square wave potentials of varying amplitudes across the cell and observed the time responses of the diffracted X-ray intensity. We used a stand-alone multi-channel scaler (MCS) in a manner similar to the method of Finnefröck et al. [7] to monitor the time response. The applied square waves each had a high potential for ~ 0.2 s and a low potential for ~ 0.2 s. The time period from one fall of the applied cell potential to the next fall was divided into many sub-intervals (or ‘channels’) each $400 \mu\text{s}$ in duration. After the applied square wave potential fell, the MCS unit began sweeping through all of the channels and incremented the respective channel counters to record the number of photons that were observed during the interval. Typical count rates were on the order of ~ 2 counts per channel per sweep. The process was repeated 500 times to accumulate a smooth distribution of counts between adjacent sub-intervals. The first 1024 intervals (corresponding to 0.4096 s) of each period were recorded. During the remaining portion of the period the computer remained idle until the square wave potential again fell. We observed the response of the system to four different applied square wave potentials:

- A) -0.506 to -0.748 to -0.506 V,
- B) -0.599 to -0.751 to -0.599 V,
- C) -0.650 to -0.752 to -0.650 V, and
- D) -0.703 to -0.750 to -0.703 V.

Only the amplitude of the applied potential was varied. The timing of the fall and the rise was not changed throughout the experiment.

3. Experimental results

We observed (Fig. 2) that the steady state scattered intensity from the $(1/2, 1/2, L)$ rod was consistent with the Ising model prediction of $S \propto (V - V_c)^{2\beta}$ for $V > V_c$. However, there was some amount of hysteresis that

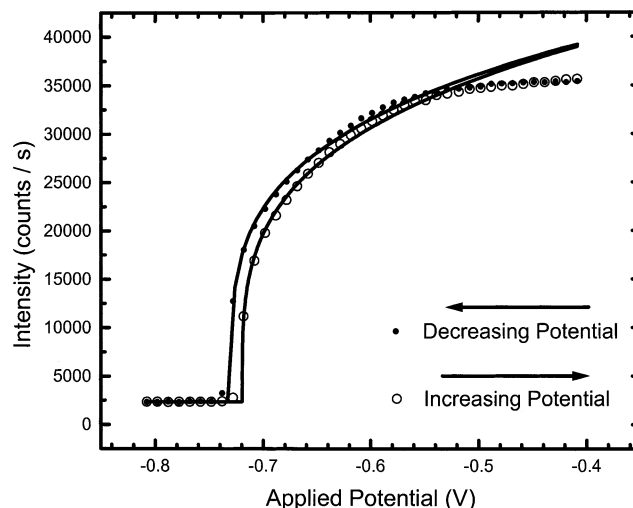


Fig. 2. Observed intensity of X-ray scattering at $(1/2, 1/2, 0.05)$. The hollow circles represent the intensity as the applied potential swept from -0.8 to -0.4 V. The solid circles represent the intensity as the applied potential swept from -0.4 to -0.8 V. Each data point was measured for 10 s. The data points from -0.5 to -0.8 V were fit to the model $S(V) = A_0(V - V_c)^{2\beta} + B_0$ in order to minimize the χ^2 value. For the increasing potential, $A_0 = 50200 \pm 600$, $V_c = -0.7303 \pm 0.0002$, $\beta = 0.129 \pm 0.003$, and $B_0 = 2350$. For the decreasing potential, $A_0 = 49400 \pm 600$, $V_c = -0.720 \pm 0.0002$, $\beta = 0.1351 \pm 0.003$, and $B_0 = 2350$.

caused the critical potential to shift up or down depending on the direction of the scan. Such sweep-dependent hysteretic effects are common in electrochemical systems, so we were not concerned that we had failed to reach thermodynamic equilibrium. The best fits shown in Fig. 2 were produced by minimizing the χ^2 value from the observed and modeled intensities for potentials from -0.8 to -0.5 V. The critical exponents of the fits were consistent with the $\beta = 1/8$ value of the 2D-Ising model. The observed critical potentials of -0.72 and -0.73 V were slightly more positive than previous observations [1], but this shift may be attributed to differences in the reference electrode. As with other critical phenomena, the Ising model only provides a good fit near the critical level. Farther away from the critical level, the model becomes less accurate. The limit of this model is seen in its failure to predict the observed saturation intensity.

When we applied a square wave that jumped across this critical potential, we observed that the transition from the disordered state to the ordered state did not immediately occur. Unfortunately the timing of the applied square wave was miscalibrated, so we later determined the times at which the wave fell and rose by finding the best possible fit to our results as discussed in the next section. Fig. 3 shows the square wave potential that we determined was applied and the response of the cell. It is significant that the intensity of the diffracted X-rays does not have a square shaped time-dependence like the applied cell potential. There are two possible explanations of this observed time delay: (a) the kinetics

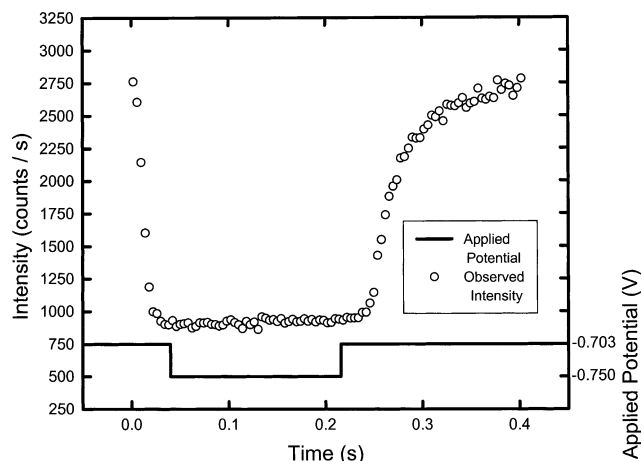


Fig. 3. The solid line shows a step potential which was applied to the Ag(001) crystal relative to the [Ag/AgCl] reference electrode. The fall time ($t_1 = 0.004$ s) and the rise time ($t_2 = 0.216$ s) of the applied potential were determined by varying their values to produce the best fit to the model discussed in Section 5. The open circles show the scattered intensity at $(1/2, 1/2, 0.05)$. High intensities correspond to the ordered phase of the adlayer, while low intensities correspond to the disordered phase. Each circle represents the average intensity recorded in ten adjacent channels of the MCS unit.

of the phase transition is delaying the transition from the disordered state to the ordered state as in the study of Finnefrock et al. [7], and (b) there is a delay associated with the transfer of the applied potential to the point on the crystal surface being observed with X-rays. We model the electrochemical cell as a RC circuit to examine the latter possibility.

4. Modeling of potential response

Our experimental measurements observed the relative ordering of the adlayer at a *localized* point on the sample crystal. The incident beam was diffracted from a small area of the sample surface. Consequently the observed intensity must depend on the relative ordering of the adlayer at the point of incidence, which in turn depends on the localized potential. In order to predict the time-dependence of this localized potential, we model the thin layer electrochemical cell as a RC circuit. The model takes into account both (a) the resistance of the electrolyte and (b) the capacitance associated with the electrical double layer. Any time delays associated with the applied potential traveling through the bulk of the electrolyte are negligible because the resistance and capacitance of the bulk are very small compared with the region of the thin layer. We, therefore, assume that the step potential is applied instantly (and equally) at all points on the edge of the crystal.

For convenience the resistivity of the electrolyte is represented by ρ , the capacitance per unit area due to the electrical double layer is represented by γ , the

thickness of the thin film of electrolyte is represented by Δz , and the radius of the crystal is represented by R . For times less than t_0 , the potential applied at the edge of the crystal is V_i . For times greater than t_0 , the applied potential is V_f . We assume that the crystal has a uniform potential of V_i at all points in its interior prior to t_0 . At time t we represent the potential at radius r and at polar angle φ by $V(r, \varphi, t)$. For $0 < r < R$ and $t > t_0$, a differential equation describing the thin layer geometry may be found by modeling the system as an array of infinitesimal resistors and capacitors. Applying Ohm's Law, charge conservation, and the definition of capacitance to this array leads to the diffusion equation:

$$\frac{1}{\kappa} \frac{\partial V}{\partial t} = \nabla^2 V \quad (1)$$

where $1/\kappa \equiv (\rho\gamma/\Delta z)$. The equation describes the diffusion of charge across the surface of the electrode. The system is subject to the boundary conditions:

$$V(r, \varphi, t < t_0) = V_i \quad (0 < r < R) \quad (2)$$

and

$$V(r = R, \varphi, t > t_0) = V_f \quad (3)$$

We solved this diffusion boundary-value problem by applying the method of separating variables [9] and observing that the solution should not depend on φ because of cylindrical symmetry. We found:

$$V(r, \varphi, t) = (V_f - V_i) \left(1 - 2 \sum_{n=1}^{\infty} \frac{J_0(\xi_n r/R)}{\xi_n \cdot J_1(\xi_n)} e^{-(\xi_n^2 \kappa / R^2)t} \right) + V_i \quad (4)$$

where $J_0(r')$ and $J_1(r')$ are the Bessel functions of the zeroth and first order and the ξ_n are the n th roots of the Bessel function $J_0(r')$.

For short times and for positions near the edge of the crystal, many terms in the expansion Eq. (4) must be included for an accurate representation. Near the edge of the crystal a simpler solution may be found by taking the limit of an infinite diameter crystal. This limit reduces the problem to a 1D case in which the distance from the edge of the crystal is represented by x . The potential is applied at position $x = 0$ at time $t = t_0$. As a result of the charge diffusion, the potential $V(x, t)$ at points 'inside' the crystal are described by Eq. (1) subject to the boundary conditions:

$$V(x, t < t_0) = V_i \quad (x > 0) \quad (5)$$

and

$$V(x = 0, t > t_0) = V_f \quad (6)$$

The solution to the 1D version of the problem may be found by applying a Laplace transform followed by an inverse transform. The result [10] is:

$$V(x, t) = (V_f - V_i) \left(1 - \operatorname{erf} \left(\frac{x}{2} \sqrt{\frac{1}{\kappa t}} \right) \right) + V_i \quad (7)$$

where $\operatorname{erf}(z)$ is the error function.

This second solution clearly has a simpler closed form, and for points near the edge of the crystal the equation is much more convenient to work with. At radius $r = 0.995R$, we used MATHEMATICA 4.0 [11] to observe that the 1D solution Eq. (7) provides a very close fit to the 2D solution produced by the first 1000 terms of the sum in Eq. (4). However, at points in the interior of the crystal the two solutions predict significantly different behavior. Fig. 4 compares these predictions. With the exception of a negative tail near zero (due to the absence of higher order terms), the first nine terms of the sum in Eq. (4) provide a good fit for points located at radius $r = 0.7R$. By setting the negative potentials of the tail to 0, a more accurate solution is generated (not shown). For this work we have used the first nine terms of the sum with all negative values being set to 0.

5. Modeling of Intensity Response

In modeling the response of the cell so far we have proposed a model that predicts the electrical potential at a localized point on the crystal. Our measurements,

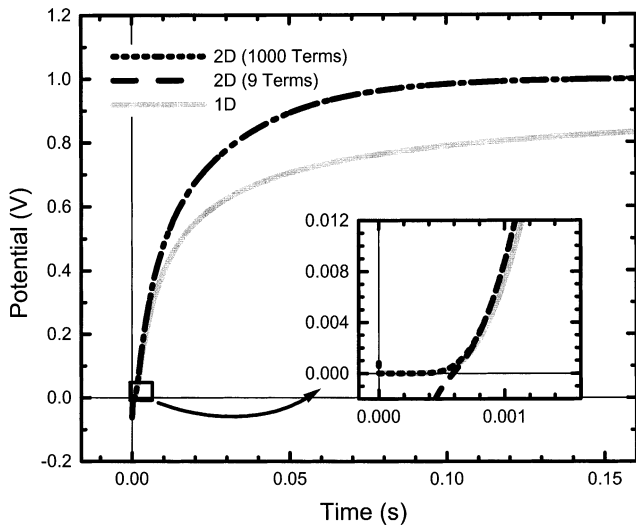


Fig. 4. The time-dependent potential responses predicted by different models at a position 1.2 mm from the edge of a crystal are shown for diffusion constant, $\kappa = 100 \text{ mm}^2 \text{ s}^{-1}$ when the applied potential jumps from 0 to 1 V. The solid gray line shows the potential predicted by the 1D model (Eq. (7)) at $x = 1.2 \text{ mm}$. The dashed black line and the dotted black line show the potential predicted by the 2D model (Eq. (4)) at radial position, $r = 2.8 \text{ mm}$ on a crystal of radius, $R = 4.0 \text{ mm}$. The dashed line uses the first ten terms of Eq. (4), while the dotted line uses the first 1000 terms of Eq. (4). The higher order terms only play a significant role at very small times corresponding to very small intensities as shown in the inset.

however, have recorded a scattered intensity. In order to relate our model to our observations, we must additionally model the scattered intensity arising from the localized potential. Before doing so we briefly point out that the scattered intensity that we want to model actually arises from the incident X-ray beam being diffracted from a stripe cutting across the crystal. Although the incident beam is square in shape, the illuminated region is rectangular because of the small incidence angle. Our model for the time-dependence of the potential is also position-dependent and predicts that the potential in the stripe of incidence is non-uniform. In order to simplify our problem, we make the approximation that the potential throughout this region takes on the value predicted at its center.

As was mentioned earlier, the steady-state scattered intensity is explained well by the 2D-Ising model in which $S = A_0(V - V_c)^{2\beta} + B_0$ for $V > V_c$. We have included the term B_0 to represent the background intensity level. A_0 is the amplitude of the power law. By recalling the observed hysteresis due to the direction of the sweep (Fig. 2), we realize that two sets of parameters will be needed to describe the intensity response: one for a rising potential and one for a falling potential. We introduce the variables A_{0r} , β_r , and V_{cr} to respectively represent the amplitude of the power law, the critical exponent, and the critical potential associated with the rising potential. The variables A_{0f} , β_f , and V_{cf} similarly represent the respective terms in the intensity response of the falling potential. We describe these intensity responses as:

$$\begin{cases} S_{\text{rise}}(V) = A_{0r}(V - V_{cr})^{2\beta_r} + B_0, & V > V_{cr} \\ S_{\text{rise}}(V) = B_0, & V < V_{cr} \end{cases} \quad (8)$$

and

$$\begin{cases} S_{\text{fall}}(V) = A_{0f}(V - V_{cf})^{2\beta_f} + B_0, & V > V_{cf} \\ S_{\text{fall}}(V) = B_0, & V < V_{cf} \end{cases} \quad (9)$$

The parameters used in fitting will depend on the sweep range and the sweep rate of the localized potential. Once suitable values for the parameters are determined, this second model will take the localized potential at a fixed point of the crystal and predict the scattered intensity that should arise.

Section 2 describes the four square-wave potentials we applied. We gathered time-dependent intensity measurements for each of these potentials. In modeling our observations, we assumed that immediately prior to an applied potential jump from V_1 to V_2 , the crystal potential was uniformly fixed at V_1 . We represented the fall time of the applied potentials with the parameter t_1 and the rise time of the applied potentials with the parameter t_2 . These two parameters were referenced to the first channel of the MCS being assigned $t = 0$. Since only the amplitudes of the applied waves were changed during the experiment, t_1 and t_2 maintained the same

values when fitting the responses of different applied potentials.

In the 2D solution Eq. (4) we used the known value $R = 4.0$ mm for the radius of the sample. To represent the center position of the incident X-rays we assigned a radius of $r = 2.8$ mm in solution Eq. (4). This value is smaller than our estimate of 3.5 mm made during our experimental set-up, but it produces a better fit in our modeling. At this off-center position, we observed that the steady-state response of the cell in the disordered phase resulted in a background intensity (B_0) of ~ 1000 counts per second. In order to find the best set of parameters for all of our observations, we first picked the observed intensity due to one of the applied potentials. We varied the parameters κ , t_1 , t_2 , and the parameters of Eqs. (8) and (9) until we had a good fit for the observed time-dependent intensity of this one applied potential. The amplitudes A_{0f} and A_{0r} were constrained so that the intensity predicted by the model at V_{high} for both S_{rise} and S_{fall} was that of the observed saturation intensity at the end of a full cycle of the applied square wave potential. We then kept the value of κ , t_1 , and t_2 , and found new values for the parameters in Eqs. (8) and (9) for each of the remaining applied potentials. After a good fit was found for each of the four applied potentials, we went back and varied κ , t_1 , and t_2 and then repeated the whole process of fitting the parameters of Eqs. (8) and (9). The process was repeated several times until we had values of κ , t_1 , and t_2 which seemed to produce good fits for all four of the applied potentials: $\kappa = 73 \text{ mm}^2 \text{ s}^{-1}$, $t_1 = 0.004 \text{ s}$, and $t_2 = 0.218 \text{ s}$. Values of the parameters A_{0f} , A_{0r} , V_{cf} , V_{cr} , β_f , and β_r in Eqs. (8) and (9) which produced good fits for each of the applied potentials are included in Table 1. Note that we have sometimes allowed the critical exponent β to deviate from the theoretical value of $1/8$. Since this provides a superior fit to the observed intensities, it suggests that under kinetic conditions, the intensity response function is different from the steady-state response function.

Fig. 5 compares the observed intensities with the intensities obtained from our model. The model successfully predicts the long time delay associated with the rising edge of the applied -0.750 to -0.703 V square

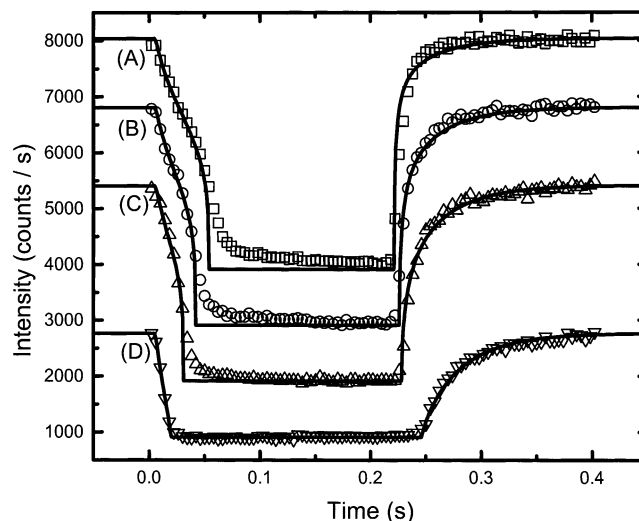


Fig. 5. The observed time-dependent intensity responses to the applied square wave potentials (A) -0.506 to -0.748 V ; (B) -0.599 to -0.751 V ; (C) -0.650 to -0.752 V ; and (D) -0.703 to -0.750 V are respectively shown by squares, circles, up triangles and down triangles. The best fits of the time-dependent intensity model incorporating the RC potential response and the Ising intensity response are shown by the black lines. For clarity, the intensities associated with the potential jump -0.650 to -0.752 V have been offset by $+1000$ counts per second. The intensities of -0.599 to -0.751 V have been offset by $+2000$ counts per second, and the intensities of -0.506 to -0.748 V have been offset by $+3000$ counts per second.

wave potential (D). However, the long tails associated with the falling edge of the square wave potentials were not explained correctly. This tailing effect can be seen directly in the steady-state potential-dependent intensity shown in Fig. 2: the Ising model predicts a sharp critical transition that was not actually observed. The observed potential-dependent tailing may be due to localized inhomogeneities or impurities within the crystal that shift the localized critical potential. When integrated, such a range of critical potentials would result in a characteristic tailing. Furthermore our assumption that the incident X-rays are diffracted from a point on the sample surface neglects the spread in potential of the actual region of diffraction. This potential range would produce an even greater tailing effect than that observed in the steady-state situation. Since the tailing effects

Table 1

The model parameters used to produce good fits to the observed time-dependent intensity responses of four applied square wave potentials

Applied square-wave potential		Fitting parameters					
V_{high} (V)	V_{low} (V)	A_{0f} (counts/s)	V_{cr} (V)	β_f	A_{0r} (counts/s)	V_{cr} (V)	β_r
-0.506	-0.748	6172	-0.705	0.125	6075	-0.718	0.125
-0.599	-0.751	6682	-0.714	0.125	8681	-0.700	0.175
-0.650	-0.752	6840	-0.718	0.125	14028	-0.712	0.250
-0.703	-0.750	20883	-0.727	0.325	65654	-0.718	0.425

The scattered intensity (S) due to a localized potential V is given by $S = A_0 (V - V_c)^{2\beta} + B_0$.

were observed, we next tried to incorporate them into the overall cell model.

In place of Eqs. (8) and (9), we defined two new numerical functions $S'_{\text{rise}}(V)$ and $S'_{\text{fall}}(V)$. These new functions respectively describe the response to the rise and the fall of the applied potential by linking each observed intensity in Fig. 2 with its adjacent neighbor by a line segment. The resulting functions map each of the ~ 40 short intervals of the measured potentials to an appropriate intensity. For each applied square wave potential (V_{high} to V_{low}), we again adjusted the relative amplitudes of $S'_{\text{rise}}(V)$ and $S'_{\text{fall}}(V)$ to ensure that these intensities at V_{high} matched the observed saturation intensity. By simply shifting these connected functions left or right (to adjust the critical potential for the respective sweep range), we were able to generate a better time response associated with the falling potential. The values of κ , t_1 , and t_2 remained the same as when using the power law fits. The fits of the numerical model to the observed intensity responses are shown in Fig. 6. As expected this model more closely predicts the observed tailing effects.

We also tried fitting our observations using the 1D model solution Eq. (7) at varying positions relative to the edge of the crystal. The results were not quite as good as those predicted by the 2D model, but the value of κ that produced the best fit was consistent. For the 2D model (Eq. (4)) we found a good fit using the value $\kappa = 73 \text{ mm}^2 \text{ s}^{-1}$ when the intensity was calculated from a point at radius 2.8 mm of a 4.0 mm radius crystal. For the 1D model we found a good fit using the value $\kappa = 119 \text{ mm}^2 \text{ s}^{-1}$ when the position $x = 1.2 \text{ mm}$ (from the edge of the cell) was used. Both values are reasonable for

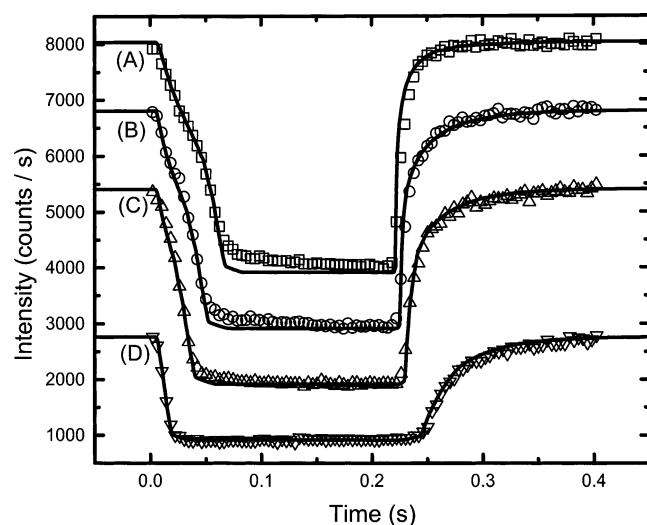


Fig. 6. The same experimental data shown in Fig. 5 are fit to numerically-defined functions (see text) to provide a more direct link to the observed steady-state intensity response. As in Fig. 5, the intensities associated with each applied potential have been offset by 1000 counts per second.

the cell we worked with. The resistivity (ρ) of our 1 M NaClO₄ solution is on the order of $\sim 0.1 \Omega \text{ m}$ [12]. We estimate the thickness (Δz) of the electrolyte film between the crystal and the polypropylene sealing film as $\sim 10 \mu\text{m}$. The capacitance per unit area (γ) near the critical potential has been observed to be on the order $\sim 100 \mu\text{F cm}^{-2}$ [13]. These estimates predict a diffusion constant $\kappa = (\Delta z / \rho \gamma)$ on the order of $\sim 100 \text{ mm}^2 \text{ s}^{-1}$. Thus our model values for κ are reasonable.

6. Conclusions

In contrast to the system studied by Finnefrock et al. [7], we have seen that the time response of the Bromide on Ag(001) electrochemical cell is primarily determined by the characteristics of its thin-layer geometry and may be modeled as a two dimensional RC circuit. The model value of the diffusion constant ($\kappa = 73 \text{ mm}^2 \text{ s}^{-1}$) is reasonable for the characteristics of the cell studied. We have also mentioned that the 1D model provides a less accurate prediction of the time-dependent intensity when the incident X-rays are diffracted from a point which is not near the edge of the crystal.

Further studies should be done in which the incident X-ray beam probes different radii (r) of the electrochemical cell to confirm the position dependence of the timed intensity response. Faster transitions should be observed near the edge of the crystal, and slower transitions should be observed near the crystal center. Such studies would allow a better characterization of the time-response in this widely used experimental geometry. The position dependence of our model suggests that the time dependence of the system may be eliminated by moving the incident X-rays to the edge of the crystal. Alternative methods of removing the time dependence of the cell have been proposed [14].

Acknowledgements

This work was supported by the NSLS under contract DEAC 02-98CH10886 and by the Frederick Seitz Materials Research Lab under contract DEFG 02-96ER45439. K. Tamura acknowledges the Japan Society for the Promotion of Science for his fellowships to do research abroad during the year 2000.

References

- [1] B.M. Ocko, J.X. Wang, T. Wandlowski, *Phys. Rev. Lett.* 79 (1997) 1511.
- [2] B.N.J. Persson, *Surf. Sci. Rep.* 15 (1992) 1.
- [3] I.K. Robinson, *Phys. Rev. B* 33 (1986) 3830.
- [4] I.K. Robinson, D.J. Tweet, *Rep. Prog. Phys.* 55 (1992) 599.
- [5] L. Onsager, *Phys. Rev.* 65 (1944) 117.

- [6] F.Y. Wu, *Rev. Mod. Phys.* 54 (1982) 235.
- [7] A.C. Finnefrock, K.L. Ringland, J.D. Brock, L.J. Buller, H.D. Abruña, *Phys. Rev. Lett.* 81 (1998) 3459.
- [8] J. Wang, B.M. Ocko, *Phys. Rev. B* 46 (1992) 10321.
- [9] G.B. Arfken, H.J. Weber, *Mathematical Methods for Physicists*, fifth ed., Harcourt/Academic Press, San Diego, CA, 2001.
- [10] J. Matthews, R.L. Walker, *Mathematical Methods of Physics*, W.A. Benjamin, New York, NY, 1970.
- [11] MATHEMATICA 4.0, Wolfram Research, Inc, Champaign, IL, 1999.
- [12] D.R. Lide (Ed.), *Handbook of Chemistry and Physics*, 81st ed., CRC Press, Boca Raton, FL, 2000.
- [13] T. Wandlowski, J.X. Wang, B.M. Ocko, *J. Electroanal. Chem.* 500 (2001) 418.
- [14] K. Tamura et al., *Electrochim. Acta* (in preparation).